



# Novel (thio)barbituric-phenoxy-*N*-phenylacetamide derivatives as potent urease inhibitors: synthesis, *in vitro* urease inhibition, and *in silico* evaluations

Saeb Sedaghati<sup>1</sup> · Homa Azizian<sup>2</sup> · Mohammad Nazari Montazer<sup>1</sup> · Maryam Mohammadi-Khanaposhtani<sup>3</sup> · Mehdi Asadi<sup>1</sup> · Fatemeh Moradkhani<sup>1</sup> · Mehdi Shafiee Ardestani<sup>4</sup> · Mohammad Sadegh Asgari<sup>5</sup> · Azadeh Yahya-Meymandi<sup>6</sup> · Mahmood Biglar<sup>7</sup> · Bagher Larijani<sup>7</sup> · Seyed Esmaeil Sadat-Ebrahimi<sup>1</sup> · Alireza Foroumadi<sup>1</sup> · Massoud Amanlou<sup>1</sup> · Mohammad Mahdavi<sup>7</sup>

Received: 2 June 2020 / Accepted: 11 August 2020  
© Springer Science+Business Media, LLC, part of Springer Nature 2020

## Abstract

A novel series of (thio)barbituric-phenoxy-*N*-phenylacetamide derivatives **7a-l** was synthesized and evaluated against *Helicobacter pylori* urease. The latter assay revealed that all the synthesized compounds **7a-l** ( $IC_{50} = 0.69 \pm 0.33$ – $2.47 \pm 0.23$   $\mu$ M) were significantly more potent than two used standard inhibitors, thiourea ( $IC_{50} = 23 \pm 0.73$   $\mu$ M) and hydroxyurea ( $IC_{50} = 100 \pm 1.7$   $\mu$ M). Docking study of the synthesized compounds demonstrated that these compounds as well fitted in the urease active site. Moreover, molecular dynamic study of the most potent compound **7d** showed that this compound created important interactions with the active site flap residues, Cys592 and His593. Furthermore, *in silico* pharmacokinetic study predicted that all the synthesized compounds are drug-like.

**Keywords** Urease · Synthesis · Barbituric acid · Docking · *In silico* · *N*-phenylacetamide

## Introduction

Urease (EC 3.5.1.5) is a metalloenzyme of amidohydrolase superfamily that catalyzes conversion of urea to ammonia and carbon dioxide and therefore plays pivotal role in nitrogen cycle [1]. In agriculture, the urea performance as efficient soil fertilizer is restricted due to environmental concerns and crops damage which is attributed to urease activity [2]. In addition,

urease has been discovered as the key virulence factor of many microorganisms such as *Helicobacter pylori* (*H. pylori*) [3]. Indeed, *H. pylori* infection leads to peptic and duodenal ulcer that could further result to gastric cancer that is the second cause of death in worldwide [4]. One of the most important ways to stop *H. pylori* activity is urease inhibitors [5]. On the other hand, there are evidences that showed microbial ureases are involved in the pathogenesis of diseases such as

**Electronic supplementary material** The online version of this article (<https://doi.org/10.1007/s11224-020-01617-6>) contains supplementary material, which is available to authorized users.

✉ Mahmood Biglar  
mbiglar@tums.ac.ir

✉ Mohammad Mahdavi  
momahdavi@tums.ac.ir

<sup>1</sup> Department of Medicinal Chemistry, Faculty of Pharmacy and Pharmaceutical Sciences Research Center, Tehran University of Medical Sciences, Tehran, Iran

<sup>2</sup> Department of Medicinal Chemistry, School of Pharmacy-International Campus, Iran University of Medical Sciences, Tehran, Iran

<sup>3</sup> Cellular and Molecular Biology Research Center, Health Research Institute, Babol University of Medical Sciences, Babol, Iran

<sup>4</sup> Department of Radiopharmacy and Medicinal Chemistry, Faculty of Pharmacy, Tehran University of Medical Sciences, Tehran, Iran

<sup>5</sup> School of Chemistry, College of Science, University of Tehran, Tehran, Iran

<sup>6</sup> Department of Chemistry, Faculty of Science, University of Birjand, Birjand, Iran

<sup>7</sup> Endocrinology and Metabolism Research Center, Endocrinology and Metabolism Clinical Sciences Institute, Tehran University of Medical Sciences, Tehran, Iran

kidney stones and pyelonephritis [6]. Therefore, discovery and development of potent and safe urease inhibitors is an important target for pharmaceutical researchers.

Barbituric acid derivatives exhibited a wide range of biological activities such as sedative, hypotensive, tranquilizing, and antibacterial [7–9]. Furthermore, several derivatives of barbituric acid with high inhibitory activity against urease had been reported [10, 11]. For example, 5-arylidene barbiturates **A** exhibited significant anti-urease activity in comparison with thiourea as standard inhibitor (Fig. 1) [12]. Moreover, compounds **B** with phenoxy moiety and compounds **C** with phenylacetamide moiety are effective inhibitors against urease (Fig. 1) [13, 14].

According to mentioned points and in continuation of our attempts for design of new and potent urease inhibitors, herein, we designed (thio)barbituric-phenoxy-*N*-phenylacetamide scaffold (Fig. 1) [15–17]. Twelve derivatives of this scaffold were synthesized via Knoevenagel condensation and were evaluated against *H. pylori* urease. *In silico* induced fit docking and molecular dynamic studies of these compounds were performed to further investigate the interaction, orientation, and conformation in the active site of urease. Furthermore, *in silico* drug-likeness and oral absorption prediction of new compounds **7a–l** were also performed.

## Experimental details

### Material and methods

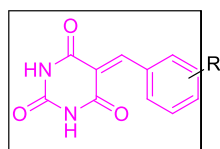
All reagents and solvents were purchased from Sigma-Aldrich (USA) and were used without further purifications. Melting points of (thio)barbituric acid-phenoxy-*N*-phenylacetamide derivatives **7a–l** were determined on Kofler hot stage

apparatus and are uncorrected. The reaction progress was monitored by thin layer chromatography (TLC); silica gel 60F<sub>254</sub> coated aluminum sheets (Merck, Germany) were visualized by ultraviolet light at wavelength of 254 and 365 nm. The IR spectra of compounds **7a–l** was recorded on Nicolet Magna FT-IR 550 spectrophotometer using KBr disks. All synthesized compounds **7a–l** were dissolved in DMSO-*d*<sub>6</sub> to obtain <sup>1</sup>H and <sup>13</sup>C NMR spectra on a Bruker FT-500 using TMS as an internal standard. Elementar Analysen System GmbH VarioEL CHN mode was used for elemental analysis of title compounds.

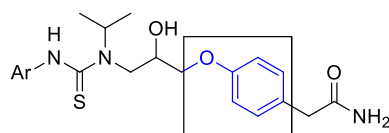
### *In vitro* urease inhibitory assay

The urease inhibitory activity of the synthesized compounds **7a–l** was determined by Berthelot spectrophotometric method [17]. In this assay, the anti-urease activity is calculated based on blue colored indophenol produced by the reaction of phenol with monochloramine, which is formed in situ through reaction of ammonia (NH<sub>3</sub>) and hypochlorite (HOCl). The absorbance of obtained indophenol was determined by a Synergy H1 Hybrid multimode microplate reader (BioTek, Winooski, VT, USA) at 625 nm.

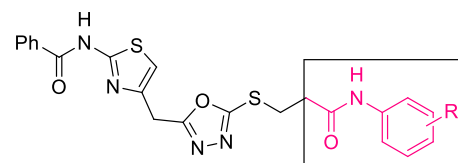
The assay mixture included urea (850 μL, 30 mM, in phosphate buffer 100 mM, pH 7.4), compounds **7a–l** (100 μL, at the concentration of 0–10 mg/ml), and phosphate buffer (100 mM, pH 7.4) with the total volume of 985 μL. Then, 15 μL of urease solution (JBU, EC 3.5.1.5, 3 mg/mL, the phosphate buffer 100 mM, pH 7.4) was added to the assay mixture, and the obtained mixture was incubated at 37 °C for 60 min. After that, the concentration of ammonia produced by the activity of uninhibited urease enzyme was determined through addition of solution A (500 μL, consist of 1% w/v phenol (5.0 g) and 0.005% w/v sodium nitroprusside



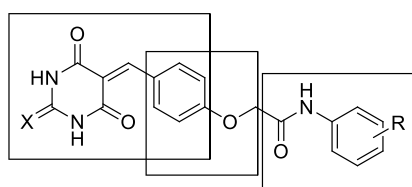
Compounds **A**: 13.0 ± 1.2 μM to not active  
Thiourea: 21.1 ± 0.3 μM



Compounds **B**: 11.73 ± 0.28–212.24 ± 0.42 μM  
Thiourea: 21.74 ± 1.76 μM



Compounds **C**: 2.58 ± 0.02–52.12 ± 0.15 μM  
Thiourea: 21.11 ± 0.12 μM



New compounds **7a–l**

Fig. 1 Design strategy for new urease inhibitors **7a–l**

(25.0 mg) in 500 mL distilled water) and solution B (500  $\mu$ L, consist of 0.5% w/v sodium hydroxide (2.5 g) and 4.2 mL sodium hypochlorite (5% chlorine) in 500 mL distilled water) and further incubated at 37 °C for 30 min. The percentage of inhibited enzyme was determined by measuring the absorbance of blue colored indophenol through the following equation:  $I (\%) = [1 - (T/C)] \times 100$ .

In the above equation,  $I (\%)$  is assigned to percent of enzyme inhibition,  $T$  (test) is assigned to the absorbance of compounds **7a-l**, positive control, and  $C$  is assigned to control which is the absorbance of the solvent in the presence of enzyme. Thiourea and hydroxyurea were used as standard urease inhibitor. The  $IC_{50}$  values were determined using PRISM 4.0 software (GraphPad, San Diego, CA, USA), and the results are shown in mean  $\pm$  standard error.

### Molecular docking study

In order to find out the interactions mode of designed molecules over urease enzyme, Maestro Molecular Modeling platform (version10.5) by Schrödinger, LLC, was performed [18]. The X-ray crystallographic structure of JBU (in complex with acetohydroxamic acid, AHA) was downloaded from the Protein Data Bank (PDB ID; 4h9m) ([www.rcsb.org](http://www.rcsb.org)). As urease is reported to be functionally active in monomeric state, all the docking studies were performed on single monomer. In addition, prosthetic group and co-factors are not directly involved in urease inhibition, so they are totally removed before docking investigation. Water molecules and co-crystallized ligands were removed from the enzymes crystallographic structures. The 2D structures of all synthesized compounds were drawn in Marvin 15.10.12.0 program (<http://www.chemaxon.com>) and converted into pdb file. The Protein Preparation Wizard and the LigPrep module were used to prepare protein and ligand structure properly [19, 20]. The missing side chains of the proteins were filled using the Prime tool, and missing residues were updated.

The accurate side-chain, backbone conformational changes or both during ligand binding at the active site of urease enzyme were predicted by IFD method using Glide software (Schrödinger LLC 2018, USA) [21]. The AHA binding site was used to generate the grid for IFD calculation. The maximum 20 poses with receptor and ligand van der Waals radii of 0.7 and 0.5, respectively, were considered. Residues within 5 Å of the AHA at the active site were refined followed by side-chain optimization. Structures whose Prime energy is more than 30 Kcal/mol are eliminated based on extra precious Glide docking.

### Molecular dynamic simulation

Molecular simulations of this study were performed using the Desmond v5.3 using Maestro interface (from Schrödinger

2018–4 suite) [22]. The appropriate pose for MD simulation procedure of the compounds was achieved by IFD method.

In order to build the system for MD simulation, the protein-ligand complexes were solvated with SPC explicit water molecules and placed in the center of an orthorhombic box of appropriate size in the periodic boundary condition. Sufficient counter-ions and a 0.15 M solution of NaCl were also utilized to neutralize the system and to simulate the real cellular ionic concentrations, respectively. The MD protocol involved minimization, pre-production, and finally production MD simulation steps. In the minimization procedure, the entire system was allowed to relax for 2500 steps by the steepest descent approach. Then the temperature of the system was raised from 0 to 300 K with a small force constant on the enzyme in order to restrict any drastic changes. MD simulations were performed via NPT (constant number of atoms; constant pressure, i.e., 1.01325 bar; and constant temperature, i.e., 300 K) ensemble. The Nose-Hoover chain method was used as the default thermostat with 1.0 ps interval and Martyna-Tobias-Klein as the default barostat with 2.0 ps interval by applying isotropic coupling style. Long-range electrostatic forces were calculated based on particle-mesh-based Ewald approach with the he cutoff radius for columbic forces set to 9.0 Å. Finally, the system subjected to produce MD simulations for 30 ns for each protein-ligand complex. During the simulation, every 1000 ps of the actual frame was stored. The dynamic behavior and structural changes of the systems were analyzed by the calculation of the root mean square deviation (RMSD) and RMSF. Subsequently, the energy-minimized structure calculated from the equilibrated trajectory system was evaluated for investigation of each ligand-protein complex interaction.

### In vitro cytotoxicity assay

*In vitro* cytotoxicity assay of the all synthesized compounds was determined against human breast cancer cell line MCF-7 cell line by MTT assay according to the previous work [23].

### In silico ADME properties of synthesized compounds

QikProp module of Schrodinger was used to calculate drug-likeness and oral absorption prediction of the synthesized compounds [24].

### General procedure for synthesis of 2-chloro-*N*-phenylacetamide derivatives **3a-g**

A mixture of aniline derivatives **1** (1 mmol) and 2-chloroacetyl chloride **2** (1 mmol) in DMF was stirred at room temperature for 30 min. At the end of the reaction (checked by TLC), the reaction mixture was diluted with cold water and poured into ice, and the obtained precipitate was filtered off.

The residue was washed with cold water to obtain pure 2-chloro-*N*-phenylacetamide derivatives **3a-g**.

### General procedure for synthesis of 2-(4-formylphenoxy)-*N*-phenylacetamide derivatives **5a-g**

A mixture of 2-chloro-*N*-phenylacetamide derivatives **3a-g** (1 mmol), 4-hydroxybenzaldehyde 1 mmol **4**, and K<sub>2</sub>CO<sub>3</sub> in DMF was heated at reflux for 3 h. After completion of reaction (checked by TLC), the reaction mixture was poured into crushed ice and filtered and washed with cold water to give pure 2-(4-formylphenoxy)-*N*-phenylacetamide derivatives **5a-g**.

### General procedure for synthesis of (thio)barbituric acid-phenoxy-*N*-phenylacetamide derivatives **7a-l**

A solution of (thio)barbituric acid **6a-b** (1 mmol) and 2-(4-formylphenoxy)-*N*-phenylacetamide derivatives **5a-g** in MeOH/EtOH (1:1, 10 mL) in presence of *p*-toluenesulfonic acid (1 mmol) as catalyst was refluxed for 8–12 h (checked by TLC). Then, the reaction mixture was filtered off, and residue was washed with cold methanol to give pure (thio)barbituric acid-phenoxy-*N*-phenylacetamide derivatives **7a-l**.

### *N*-phenyl-2-(4-((2,4,6-trioxotetrahydropyrimidin-5(2H)-ylidene)methyl)phenoxy) acetamide (**7a**)

Yield 92%; Cream powder; mp 185–190 °C. IR (KBr, cm<sup>-1</sup>):  $\nu = 3338, 3026, 2961, 1728$ , <sup>1</sup>H NMR (500 MHz, DMSO-*d*<sub>6</sub>)  $\delta$  10.00 (s, 2H, 2NH), 9.58 (s, 1H, NH-amide), 8.17 (s, 1H, CH-vinyl), 7.34–7.30 (m, 3H, Ar), 7.06 (dd,  $J = 13.5, 7.9$  Hz, 3H, Ar), 4.58 (s, 2H, CH<sub>2</sub>). <sup>13</sup>C NMR (126 MHz, DMSO-*d*<sub>6</sub>)  $\delta$  157.92, 151.11, 138.84, 138.13, 130.27, 129.78, 129.19, 129.10, 128.05, 120.30, 120.16, 115.18, 114.14, 69.03. Anal. Calcd for C<sub>19</sub>H<sub>15</sub>N<sub>3</sub>O<sub>5</sub>: C, 62.46; H, 4.14; N, 11.50. Found: C, 62.49; H, 4.12; N, 11.55.

### *N*-(4-fluorophenyl)-2-(4-((2,4,6-trioxotetrahydropyrimidin-5(2H)-ylidene)methyl)phenoxy) acetamide (**7b**)

Yield 87%; Cream powder; mp 208–213 °C. IR (KBr, cm<sup>-1</sup>):  $\nu = 3327, 3020, 2966, 1731$ . <sup>1</sup>H NMR (500 MHz, DMSO-*d*<sub>6</sub>)  $\delta$  9.88 (s, 2H, 2NH), 9.76 (s, 1H, NH-amide), 8.30 (s, 1H, CH-vinyl) 7.89 (d,  $J = 8.8$  Hz, 2H, Ar), 7.64 (dd,  $J = 8.9, 5.0$  Hz, 2H, Ar), 7.20–7.14 (m, 4H, Ar), 4.84 (s, 2H, CH<sub>2</sub>); <sup>13</sup>C NMR (126 MHz, DMSO-*d*<sub>6</sub>)  $\delta$  191.79, 166.27, 163.17, 135.13, 135.11, 132.20, 130.58, 122.04, 121.98, 115.89, 115.71, 115.65, 67.51. Anal. Calcd for C<sub>19</sub>H<sub>14</sub>FN<sub>3</sub>O<sub>5</sub>: C, 59.53; H, 3.68; N, 10.96. Found: C, 59.48; H, 3.65; N, 10.94.

### *N*-(2,4-difluorophenyl)-2-(4-((4,6-dioxo-2-thioxotetrahydropyrimidin-5(2H)-ylidene)methyl)phenoxy) acetamide (**7c**)

Yield 86%; Cream powder; mp 201–207 °C. IR (KBr, cm<sup>-1</sup>):  $\nu = 3337, 3023, 2966, 1681$ , <sup>1</sup>H NMR (500 MHz, DMSO-*d*<sub>6</sub>)  $\delta$  9.48 (s, 1H, 2NH), 8.37 (s, 2H, NH-amide), 8.20 (s, 1H, CH-vinyl), 7.89 (d,  $J = 8.4$  Hz, 2H, Ar), 7.75 (q,  $J = 8.9$  Hz, 1H, Ar), 7.38–7.30 (m, 1H, Ar), 7.18 (d,  $J = 8.6$  Hz, 2H, Ar), 7.08 (t,  $J = 7.9$  Hz, 1H, Ar), 4.91 (s, 2H, CH<sub>2</sub>); <sup>13</sup>C NMR (126 MHz, DMSO-*d*<sub>6</sub>)  $\delta$  177.41, 174.48, 166.87, 163.09, 160.69, 158.88, 155.08, 150.65, 132.19, 130.61, 126.95, 126.88, 122.27, 122.15, 115.64, 111.79, 111.59, 104.95, 104.75, 104.54, 67.28. Anal. Calcd for C<sub>19</sub>H<sub>13</sub>F<sub>2</sub>N<sub>3</sub>O<sub>4</sub>: C, 54.67; H, 3.14; N, 10.07. Found: C, 54.61; H, 3.12; N, 10.09.

### *N*-(2,3-dichlorophenyl)-2-(4-((2,4,6-trioxotetrahydropyrimidin-5(2H)-ylidene)methyl)phenoxy) acetamide (**7d**)

Yield 89%; Cream powder; mp 178–180 °C. IR (KBr, cm<sup>-1</sup>):  $\nu = 3323, 3018, 2967, 1733$ . <sup>1</sup>H NMR (500 MHz, DMSO-*d*<sub>6</sub>)  $\delta$  10.50 (s, 1H, NH-amide), 9.92 (s, 2H, 2NH), 9.27 (s, 1H, CH-vinyl), 8.36 (d,  $J = 8.6$  Hz, 1H, Ar), 7.91 (d,  $J = 8.6$  Hz, 1H, Ar), 7.52–7.49 (m, 1H, Ar), 7.21 (d,  $J = 9.5$  Hz, 1H, Ar), 7.14 (d,  $J = 8.4$  Hz, 1H, Ar), 7.08 (d,  $J = 8.4$  Hz, 1H, Ar), 6.98 (d,  $J = 6.8$  Hz, 1H, Ar), 4.95 (s, 2H, CH<sub>2</sub>); <sup>13</sup>C NMR (126 MHz, DMSO-*d*<sub>6</sub>)  $\delta$  191.83, 166.95, 162.88, 137.58, 136.57, 132.39, 132.22, 130.72, 128.64, 127.62, 125.04, 115.72, 115.03, 67.38. Anal. Calcd for C<sub>19</sub>H<sub>13</sub>Cl<sub>2</sub>N<sub>3</sub>O<sub>5</sub>: C, 52.55; H, 3.02; N, 9.68. Found: C, 52.53; H, 3.07; N, 9.63.

### *N*-(3-chloro-2-methylphenyl)-2-(4-((2,4,6-trioxotetrahydropyrimidin-5(2H)-ylidene)methyl)phenoxy) acetamide (**7e**)

Yield 91%; Cream powder; mp 181–183 °C. IR (KBr, cm<sup>-1</sup>):  $\nu = 3329, 3020, 2961, 1722$ . <sup>1</sup>H NMR (500 MHz, DMSO-*d*<sub>6</sub>)  $\delta$  9.89 (s, 2H, 2NH), 8.99 (s, 1H, NH-amide), 8.26 (s, 1H, CH-vinyl), 7.91 (d,  $J = 8.4$  Hz, 2H, Ar), 7.35–7.32 (m, 2H, Ar), 7.22 (t,  $J = 8.2$  Hz, 3H, Ar), 4.90 (s, 2H, CH<sub>2</sub>), 2.20 (s, 3H, CH<sub>3</sub>); <sup>13</sup>C NMR (126 MHz, DMSO-*d*<sub>6</sub>)  $\delta$  191.82, 166.75, 163.08, 137.49, 134.23, 132.20, 131.48, 130.63, 127.36, 127.02, 125.40, 115.70, 67.44, 15.51. Anal. Calcd for C<sub>20</sub>H<sub>16</sub>ClN<sub>3</sub>O<sub>5</sub>: C, 58.05; H, 3.90; N, 10.15. Found: C, 58.01; H, 3.87; N, 10.18.

### 2-(4-((4,6-dioxo-2-thioxotetrahydropyrimidin-5(2H)-ylidene)methyl)phenoxy)-*N*-phenylacetamide (**7f**)

Yield 94%; Cream powder; 212–214 °C. IR (KBr, cm<sup>-1</sup>):  $\nu = 3326, 3019, 2961, 1687$ . <sup>1</sup>H NMR (500 MHz, DMSO-*d*<sub>6</sub>)  $\delta$  10.17 (s, 2H, 2NH), 9.61 (s, 1H, NH-amide), 8.09 (s, 1H, CH-

vinyl), 7.91 (d,  $J = 7.7$  Hz, 2H, Ar), 7.64 (d,  $J = 6.8$  Hz, 2H, Ar), 7.37–7.29 (m, 2H, Ar), 7.20 (d,  $J = 7.6$  Hz, 2H, Ar), 7.10 (s, 1H, Ar), 4.87 (s, 2H, CH<sub>2</sub>); <sup>13</sup>C NMR (126 MHz, DMSO-*d*<sub>6</sub>)  $\delta$  191.81, 166.30, 163.24, 138.79, 132.55, 132.21, 130.57, 129.24, 129.15, 124.23, 120.31, 120.14, 115.65, 67.56. Anal. Calcd for C<sub>19</sub>H<sub>15</sub>N<sub>3</sub>O<sub>4</sub>S: C, 59.83; H, 3.96; N, 11.02. Found: C, 59.84; H, 3.96; N, 11.08.

**2-(4-((4,6-dioxo-2-thioxotetrahydropyrimidin-5(2H)-ylidene)methyl)phenoxy)-*N*-(4-fluorophenyl)acetamide (7g)**

Yield 87%; Cream powder; mp 174–176 °C. IR (KBr, cm<sup>-1</sup>):  $\nu = 3334, 3028, 2966, 1677$ . <sup>1</sup>H NMR (500 MHz, DMSO-*d*<sub>6</sub>)  $\delta$  10.22 (s, 2H, 2NH), 9.76 (s, 1H, NH-amide), 8.18 (s, 1H, CH-vinyl), 7.89 (d,  $J = 8.7$  Hz, 2H, Ar), 7.65 (dd,  $J = 8.9, 5.0$  Hz, 2H, Ar), 7.23–7.11 (m, 4H, Ar), 4.85 (s, 2H, CH<sub>2</sub>); <sup>13</sup>C NMR (126 MHz, DMSO-*d*<sub>6</sub>)  $\delta$  191.81, 166.27, 163.17, 135.15, 132.21, 130.60, 122.05, 121.99, 115.90, 115.72, 115.66, 67.52. Anal. Calcd for C<sub>19</sub>H<sub>14</sub>FN<sub>3</sub>O<sub>4</sub>S: C, 57.14; H, 3.53; N, 10.52. Found: C, 57.11; H, 3.57; N, 10.59.

***N*-(2,4-difluorophenyl)-2-(4-((4,6-dioxo-2-thioxotetrahydropyrimidin-5(2H)-ylidene)methyl)phenoxy)acetamide (7h)**

Yield 91%; Cream powder; mp 211–213 °C. IR (KBr, cm<sup>-1</sup>):  $\nu = 3334, 3019, 2958, 1674$ . <sup>1</sup>H NMR (500 MHz, DMSO-*d*<sub>6</sub>)  $\delta$  10.19 (s, 2H, 2NH), 9.48 (s, 1H, NH-amide), 8.20 (s, 1H, CH-vinyl), 7.89 (d,  $J = 8.4$  Hz, 2H, Ar), 7.75 (q,  $J = 8.9$  Hz, 1H, Ar), 7.38–7.30 (m, 1H, Ar), 7.18 (d,  $J = 8.6$  Hz, 2H, Ar), 7.08 (t,  $J = 7.9$  Hz, 1H, Ar), 4.91 (s, 2H); <sup>13</sup>C NMR (126 MHz, DMSO-*d*<sub>6</sub>)  $\delta$  191.80, 166.87, 163.09, 132.19, 130.61, 126.95, 126.88, 122.27, 122.15, 115.64, 111.79, 111.59, 104.95, 104.75, 104.54, 67.28. Anal. Calcd for C<sub>19</sub>H<sub>13</sub>F<sub>2</sub>N<sub>3</sub>O<sub>4</sub>S: C, 54.67; H, 3.14; N, 10.07. Found: C, 54.63; H, 3.13; N, 10.06.

***N*-(2-chlorophenyl)-2-(4-((4,6-dioxo-2-thioxotetrahydropyrimidin-5(2H)-ylidene)methyl)phenoxy)acetamide (7i)**

Yield 88%; Cream powder; mp 182–184 °C. IR (KBr, cm<sup>-1</sup>):  $\nu = 3335, 3023, 2964, 1682$ . <sup>1</sup>H NMR (500 MHz, DMSO-*d*<sub>6</sub>)  $\delta$  10.38 (s, 2H, 2NH), 9.42 (s, 1H, NH-amide), 8.65 (s, 1H, CH-vinyl), 7.84 (dd,  $J = 14.9, 8.3$  Hz, 3H, Ar), 7.53 (d,  $J = 8.2$  Hz, 1H, Ar), 7.36 (t,  $J = 7.7$  Hz, 1H, Ar), 7.23 (t,  $J = 7.6$  Hz, 1H, Ar), 7.15 (d,  $J = 8.6$  Hz, 2H, Ar), 4.87 (s, 2H, CH<sub>2</sub>); <sup>13</sup>C NMR (126 MHz, DMSO-*d*<sub>6</sub>)  $\delta$  190.79, 165.86, 162.09, 131.18, 129.61, 125.93, 121.17, 114.64, 110.59, 108.13, 103.73, 66.28. Anal. Calcd for C<sub>19</sub>H<sub>14</sub>ClN<sub>3</sub>O<sub>4</sub>S: C, 54.88; H, 3.39; N, 10.10. Found: C, 54.83; H, 3.34; N, 10.11.

***N*-(2,3-dichlorophenyl)-2-(4-((4,6-dioxo-2-thioxotetrahydropyrimidin-5(2H)-ylidene)methyl)phenoxy)acetamide (7j)**

Yield 93%; Cream powder; mp 190–192 °C. IR (KBr, cm<sup>-1</sup>):  $\nu = 3334, 3021, 2967, 1674$ . <sup>1</sup>H NMR (500 MHz, DMSO-*d*<sub>6</sub>)  $\delta$  10.50 (s, 2H, 2NH), 9.43 (s, 1H, NH-amide), 8.14 (s, 2H, CH-vinyl), 7.91 (d,  $J = 8.6$  Hz, 2H, Ar), 7.28 (d,  $J = 8.3$  Hz, 2H, Ar), 7.22 (d,  $J = 8.6$  Hz, 2H, Ar), 7.08 (d,  $J = 8.5$  Hz, 2H, Ar), 4.95 (s, 2H, CH<sub>2</sub>); <sup>13</sup>C NMR (126 MHz, DMSO-*d*<sub>6</sub>)  $\delta$  191.83, 167.25, 166.92, 136.56, 132.22, 129.48, 128.64, 127.33, 125.03, 124.39, 115.72, 114.25, 67.38. Anal. Calcd for C<sub>19</sub>H<sub>13</sub>Cl<sub>2</sub>N<sub>3</sub>O<sub>4</sub>S: C, 50.68; H, 2.91; N, 9.33. Found: C, 50.74; H, 2.96; N, 9.34.

***N*-(3-bromophenyl)-2-(4-((4,6-dioxo-2-thioxotetrahydropyrimidin-5(2H)-ylidene)methyl)phenoxy)acetamide (7k)**

Yield 90%; Cream powder; mp 200–203 °C. IR (KBr, cm<sup>-1</sup>):  $\nu = 3335, 3021, 2965, 1680$ . <sup>1</sup>H NMR (500 MHz, DMSO-*d*<sub>6</sub>)  $\delta$  10.33 (s, 2H, 2NH), 9.71 (s, 1H, NH-amide), 8.20 (s, 1H, CH-vinyl), 7.97 (s, 1H, Ar), 7.89 (d,  $J = 8.6$  Hz, 2H, Ar), 7.57 (d,  $J = 7.3$  Hz, 1H, Ar), 7.29 (d,  $J = 7.9$  Hz, 2H, Ar), 7.19 (d,  $J = 8.7$  Hz, 2H, Ar), 4.87 (s, 2H, CH<sub>2</sub>); <sup>13</sup>C NMR (126 MHz, DMSO-*d*<sub>6</sub>)  $\delta$  191.80, 166.75, 163.12, 162.83, 140.35, 132.20, 132.05, 131.26, 130.61, 129.91, 126.84, 122.44, 121.97, 118.89, 115.66, 67.45. Anal. Calcd for C<sub>19</sub>H<sub>14</sub>BrN<sub>3</sub>O<sub>4</sub>S: C, 49.58; H, 3.07; N, 9.13. Found: C, 49.54; H, 3.08; N, 9.08.

***N*-(3-chloro-2-methylphenyl)-2-(4-((4,6-dioxo-2-thioxotetrahydropyrimidin-5(2H)-ylidene)methyl)phenoxy)acetamide (7l)**

Yield 87%; Cream powder; mp 196–198 °C. IR (KBr, cm<sup>-1</sup>):  $\nu = 3334, 3016, 2963, 1688$ . <sup>1</sup>H NMR (500 MHz, DMSO-*d*<sub>6</sub>)  $\delta$  10.23 (s, 2H, 2NH), 9.14 (s, 1H, NH-amide), 8.20 (s, 1H, CH-vinyl), 7.94–7.87 (m, 2H, Ar), 7.35–7.28 (m, 2H, Ar), 7.25–7.16 (m, 3H, Ar), 4.89 (s, 2H, CH<sub>2</sub>), 2.20 (s, 3H, CH<sub>3</sub>); <sup>13</sup>C NMR (126 MHz, DMSO-*d*<sub>6</sub>)  $\delta$  190.83, 166.25, 165.92, 135.56, 131.83, 131.22, 128.48, 127.64, 126.33, 124.03, 123.39, 114.72, 113.25, 66.38, 10.59. Anal. Calcd for C<sub>20</sub>H<sub>16</sub>ClN<sub>3</sub>O<sub>4</sub>S: C, 55.88; H, 3.75; N, 9.77. Found: C, 55.86; H, 3.71; N, 9.79.

## Results and discussion

### Chemistry

The synthetic pathway for (thio)barbituric acid-phenoxy-*N*-phenylacetamide derivatives **7a-l** was depicted in Scheme 1. It started with the reaction between aniline derivatives **1a-g**

and 2-chloroacetyl chloride **2** in DMF to give 2-chloro-*N*-phenylacetamide derivatives **3a-g**. The latter compounds reacted with 4-hydroxybenzaldehyde **4** in the presence of  $K_2CO_3$  in DMF to produce 2-(4-formylphenoxy)-*N*-phenylacetamide derivatives **5a-g**. Finally, desired compounds **7a-l** were obtained from a Knoevenagel condensation between formaldehyde derivatives **5a-g** and barbituric acid derivatives **6a-b**.

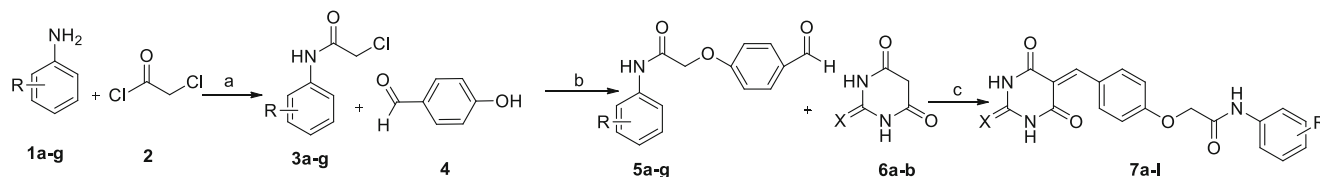
### In vitro urease inhibitory activity

Urease inhibitory activity of all the synthesized (thio)barbituric acid-phenoxy-*N*-phenylacetamide derivatives **7a-l** was determined against *H. pylori* urease. As can be seen in Table 1, compounds **7a-l** with  $IC_{50}$  values =  $0.69 \pm 0.33$  to  $2.47 \pm 0.23$   $\mu M$  exhibited excellent inhibitory activities against urease in comparison with two used standard inhibitors hydroxyurea and thiourea with  $IC_{50}$ s  $100 \pm 1.7$  and  $23 \pm 0.73$ , respectively.

Structurally, synthesized compounds **7a-l** can be divided to two series: barbituric acid derivatives **7a-e** and thio-barbituric acid derivatives **7f-l**. In each series, substituent on phenyl ring of *N*-phenylacetamide moiety was altered to optimize the urease inhibitory activity.

Among the barbituric acid derivatives, the most potent compound was compound **7d** with 2,3-dichloro substituents on *N*-phenylacetamide moiety. This compound was also the most potent compound among all the synthesized compounds. Replacement of 2-chloro substituent of this compound with 2-methyl substituent, as in compound **7e**, led to a significant decrease in inhibitory activity. The second potent compound in this series was 2,4-difluoro derivative **7c**. Removing the 2-fluoro substituent of this compound slightly diminished inhibitory activity as observed in compound **7b**. Moreover, un-substituted derivative **7a** has a slightly reduced inhibitory activity compared with 4-fluoro derivative **7b**.

The most potent compound among the thio-barbituric acid derivatives **7f-l**, was 4-fluoro derivative **7g** while the weakest compound in this series was the un-substituted compound **7f**. The introduction of second fluorine atom onto the 2-position of compound **7g**, as compound **7h**, led to a moderate decrease in inhibitory activity. Moreover, the introduction of 2-chloro, 2,3-dichloro, 3-bromo or 2-methyl-3-chloro on phenyl ring of *N*-phenylacetamide moiety did not improve anti-urease potency as observed in compounds **7i-l**.



**Scheme 1** Synthesis procedure for desired compounds **7a-l**: (a) DMF, room temperature, 30 min; (b)  $K_2CO_3$ , DMF, reflux, 2 h; (c) *p*-TsOH, MeOH/EtOH, reflux, 8–12 h

The comparison of urease inhibitory activity of barbituric acid derivatives with their corresponding thio-barbituric acid analogs revealed that barbituric acid analogs **7a**, **7c**, and **7d** respectively with un-substituted, 2,4-difluoro, and 2,3-dichloro-phenylacetamide moiety were more active than their thio-barbituric acid analogs **7f**, **7h**, and **7j**. In contrast, urease inhibitory activity of 4-fluoro and 2-methyl-3-chloro derivatives **7b** and **7e** of barbituric acid series was less than their thio-barbituric acid analogs **7g** and **7l**.

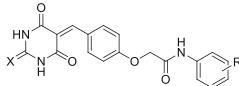
### Docking study

In order to investigate the interaction modes of the synthesized compounds **7a-l** in the active site of urease, docking study was carried out on Jack bean urease (JBU, pdb ID: 4h9m) [17]. Urease inhibitor acetohydroxamic acid (AHA) is bounded to active site of JBU.

The applied docking procedure reliability was validated by re-docking of AHA over JBU based on glide docking procedure. The docked conformation corresponding to the lowest glide energy was selected as the most possible binding modes. The root mean square deviation (RMSD) was calculated for each ligand to measure the docking prediction accuracy. The pose was counted optimal if its RMSD was found to be less than 2 Å. The RMSD of the re-docked conformations of AHA over JBU was 1.02 Å (Fig. 2), which is considered successfully docked.

The performed docking procedure was then applied to evaluate the interaction between newly synthesized compounds, **7a-l** over the JBU active site in comparison with thiourea as a reference urease inhibitor. The top scoring pose of all compounds was analyzed inside the binding site of JBU. In the binding model, all the compounds are successfully occupied in the bi-nickel active site cavity. Figure 3a shows that the fitting-in mechanism of barbituric acid and thio-barbiturate moiety in the active site of the enzyme is quite similar. The (thio)barbituric acid ring tends to orient toward the two nickel atoms through the ionized N ( $N^-$ ) and the carbonyl group at C<sub>4</sub> position of the (thio)barbiturate ring (Fig. 3b) which is similar to the behavior of the carbonyl oxygens in the AHA.

Additionally, Fig. 3 b shows that thio-barbituric acid ring appears to make some distance deviation from Ni-Ni center which caused as a result of steric effect of the sulfur atom.

**Table 1** Urease inhibitory activities of (thio)barbituric acid-phenoxy-*N*-phenylacetamide derivatives **7a-l**


Compound	X	R	IC <sub>50</sub> (μM) <sup>a</sup>	Compound	X	R	IC <sub>50</sub> (μM) <sup>b</sup>
<b>7a</b>	O	H	1.62 ± 0.14	<b>7h</b>	S	2,4-Difluoro	1.72 ± 0.41
<b>7b</b>	O	4-F	1.48 ± 0.09	<b>7i</b>	S	2-Cl	1.61 ± 0.18
<b>7c</b>	O	2,4-Difluoro	1.29 ± 0.18	<b>7j</b>	S	2,3-Dichloro	2.21 ± 0.52
<b>7d</b>	O	2,3-Dichloro	0.69 ± 0.33	<b>7k</b>	S	3-Br	2.33 ± 0.28
<b>7e</b>	O	2-CH <sub>3</sub> -3-Cl	1.75 ± 0.17	<b>7l</b>	S	2-CH <sub>3</sub> -3-Cl	1.59 ± 0.25
<b>7f</b>	S	H	2.47 ± 0.23	Hydroxyurea	-	-	100 ± 1.7
<b>7g</b>	S	4-F	1.19 ± 0.14	Thiourea	-	-	23 ± 0.73

On the other hand, the phenoxy-*N*-phenylacetamide moiety adapts by flexible conformation in the large hydrophobic opening of the active site flap pocket (Fig. 3c).

The molecular interactions of the best conformational pose and energy-valued docked complex of compounds **7d**, **7b**, **7g**, and **7c** are illustrated in Fig. 4.

Figure 4 a shows barbituric acid ring of compound **7d** tightly coordinated along the metal bi-nickel center and further stabilized by H-bond interaction with His492 and Asp633. At the

middle part of the molecule, the benzylidene group formed hydrophobic interaction through Cys592. Finally, the amide group at the tail part of the compound formed H-bond with His593, which consequently oriented the attached 2,3-dichloro phenyl group in front of the active site flap entrance.

Compounds **7b**, **7g**, and **7c** depict similar orientation and interaction to **7d** (metal coordination forming through (thio)barbituric acid ring, H-bond with Cys592 and His593) (Fig. 4 b, c, and d).

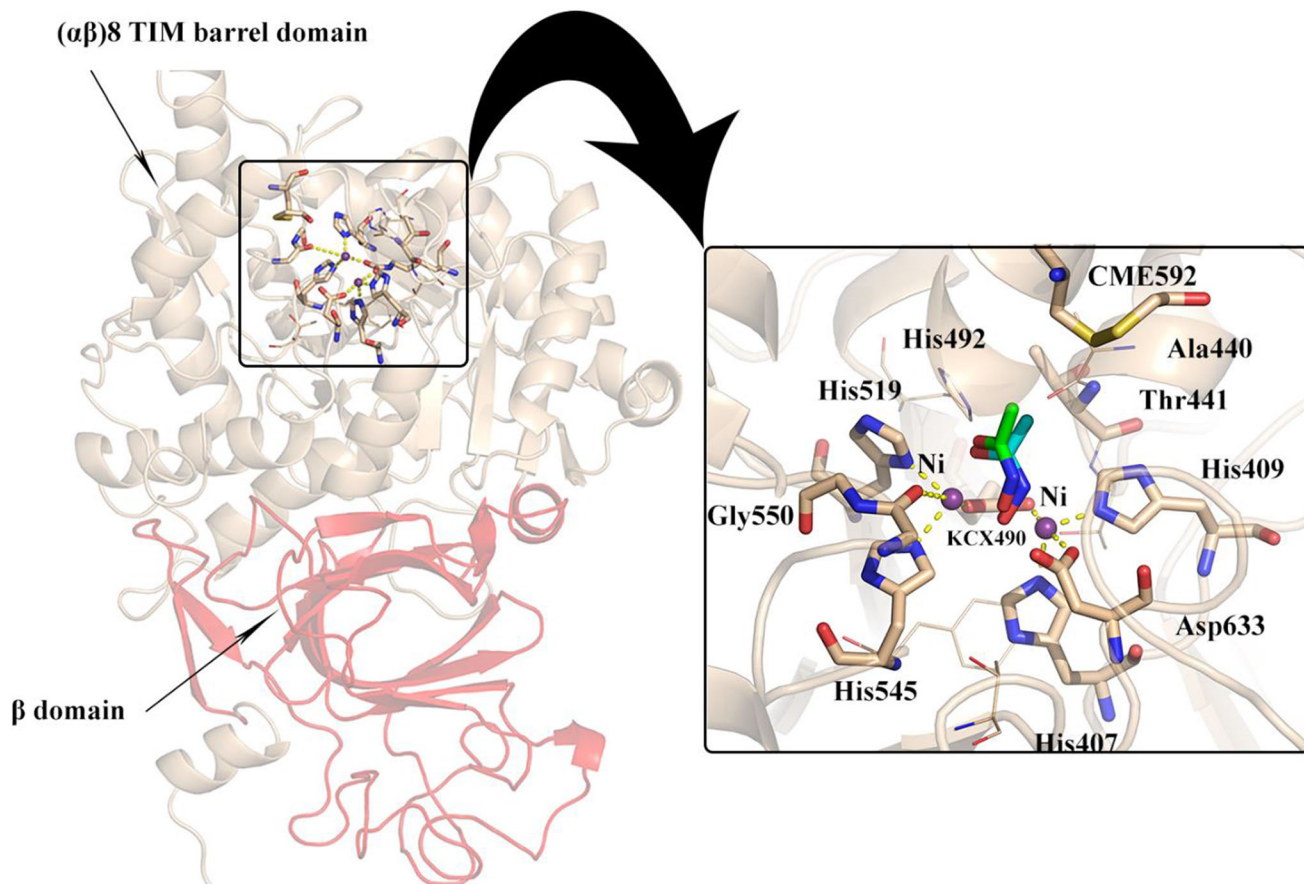


**Fig. 2** The location of JBU active site over C-terminal (αβ)<sub>8</sub> TIM barrel domain, close-up representation of active site, the AHA co-crystallized, and the corresponding re-docked form are represented in green and cyan color, respectively

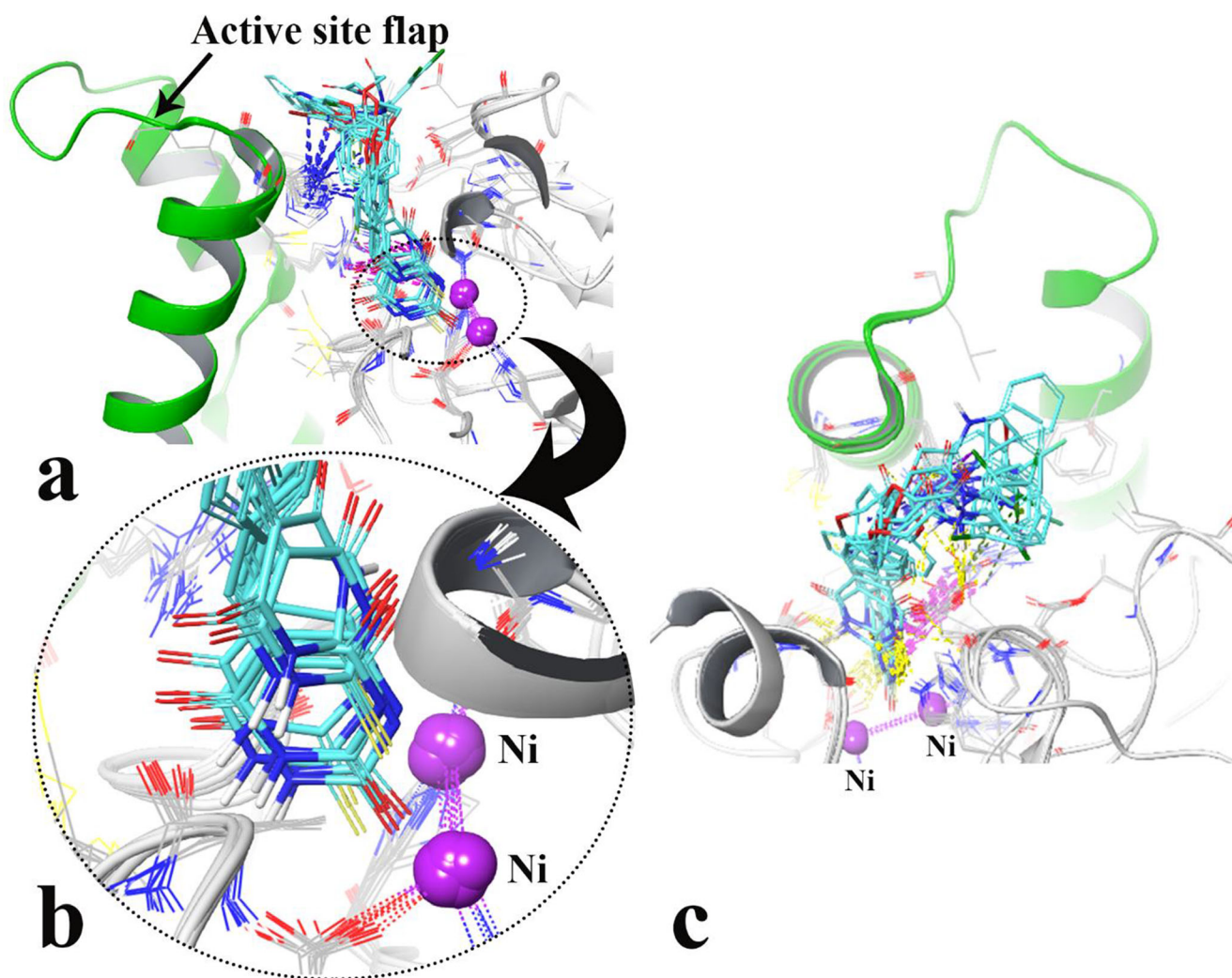


**Fig. 3** Representation of the compounds docking poses over the active site: side view representation (a), close-up illustration of (thio)barbiturate ring relative to the bi nuclear center (b), and upside view of the active site

It is noteworthy that Cys592 and His593 are of the key residues in the urease active site. Ligand interacting with these residues seems to be the most important for urease inhibition because of decreasing the flexibility of mobile flap covering the active site entrance followed by inhibiting the ureolytic activity.

### Molecular dynamic study

In addition, to understand dynamics behavior and the detailed interactions of the most potent compound **7d** and compare it with thiourea as urease standard inhibitor, molecular dynamic (MD) simulation was performed. RMSF, which refers to the fluctuation of the C $\alpha$  atom coordinates from its average position throughout the simulation, indicates the flexibility of protein backbone structure. Loops with loosely organized structure have high RMSF value, while helixes and sheets represent lower RMSF value.

which shows the orientation of the phenoxy-*N*-phenylacetamide relative to the active site flap (colored in green color) (c)

Based on crystal structures of the ureases, besides the conserved residues in the active site, most of ureases share conserved residues that make up the mobile flap [25], which covers the active site. In JBU, the residues comprising the mobile flap are 590–606 on  $\alpha$  subunit part of the enzyme. Comparing RMSF values of urease-compound complexes shows that the residues of the flap region covering the active site, 590–606, would have significantly lower RMSF value in urease-compound **7d** rather than urease-thiourea complex (Fig. 5). Consequently, compound **7d** tightly anchoring the helix-turn-helix motif over the active-site cavity reduces the flexibility of flap residue (590–609) by interacting with key amino acid residues and results in the inhibition of urease activity.

In order to study the behavior of the active site covering flap over the course of the MD simulation, the distances between Ile599 at the tip of the flap and Ala440 at the entrance of active site channel in the urease-compound complexes are

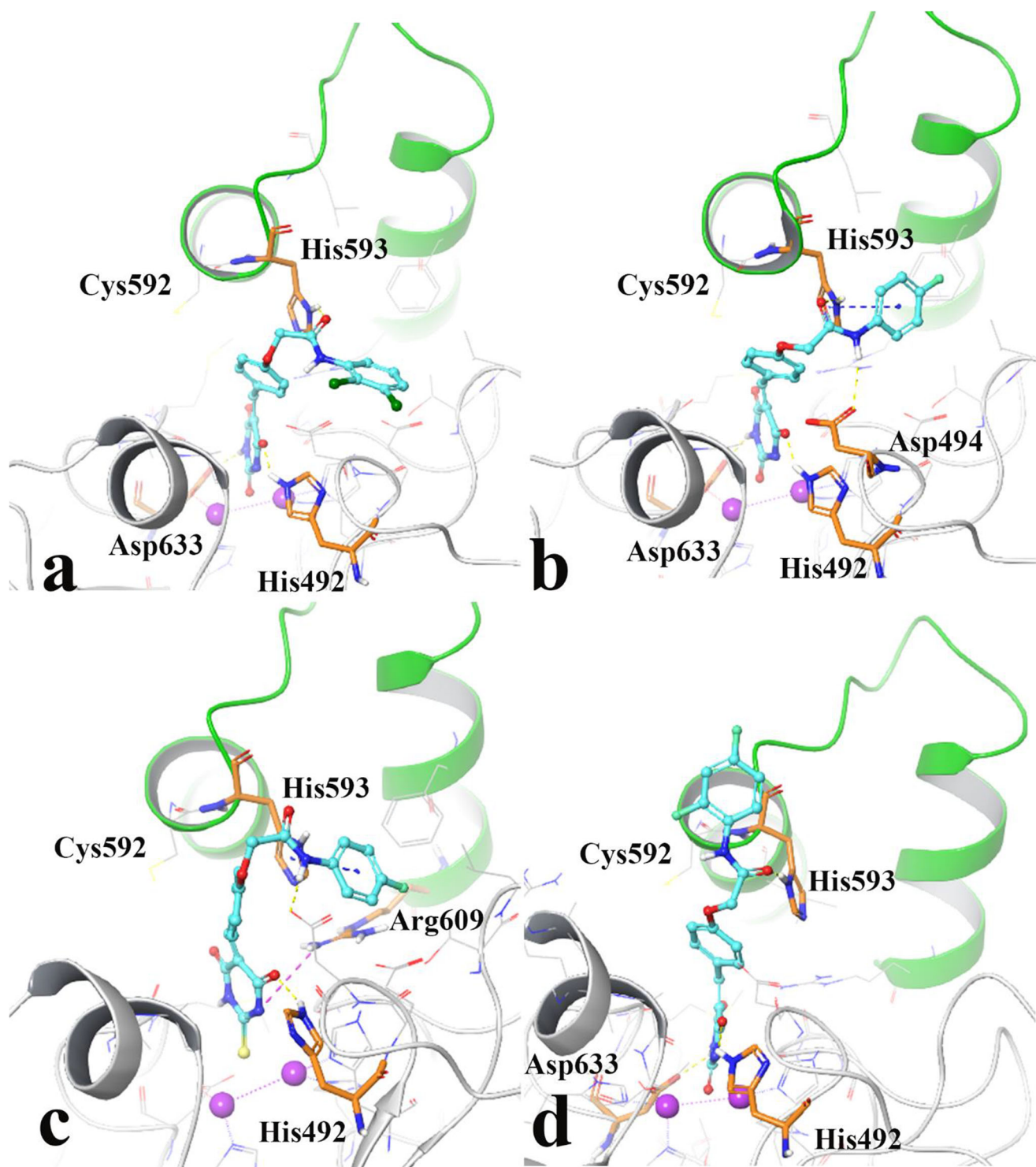
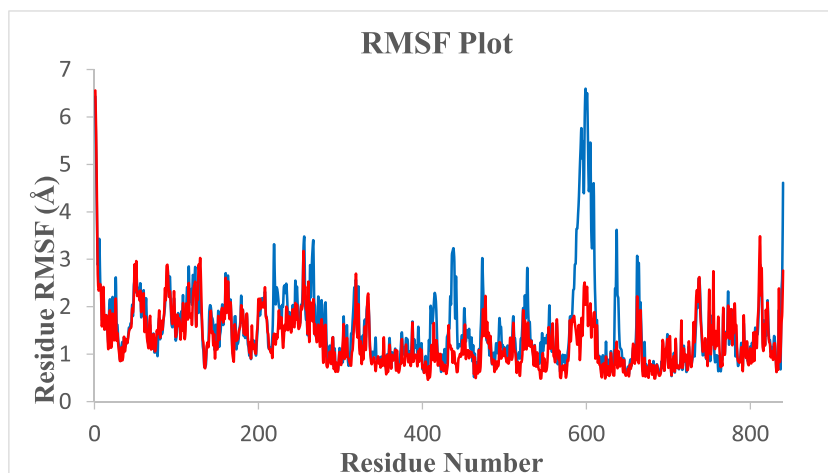


**Fig. 4** 2D representation of ligand-residue interactions of compound **7d** (a), compound **7b** (b), compound **7g** (c), and compound **7c** (d) over urease active site. Active site flap colored in green

analyzed. Figure 6 a displays representative Ile599-Ala440 separations for the urease-compound complex. In the thiourea bound-state, the separation of these residues is about 32 Å corresponding as open flap conformation, while in the case of compound **7d**, this distance varies only slightly oscillating

within 26 Å, respectively, which is related to the close flap conformation (Fig. 6b). Based on the closed flap conformation, it is proposed that compound **7d** inhibits urease activity by stabilizing the reaction intermediate during the ureolytic reaction [26].

**Fig. 5** RMSF of the urease C $\alpha$  in complexed with thiourea (colored in blue) and compounds **7d** (colored in red) for over 30 ns MD simulation time



### *In vitro* cytotoxicity assay

*In vitro* cytotoxicity of the synthesized compounds **7a–l** was evaluated against breast cancer cell line MCF-7 by MTT assay [23]. This assay revealed that at 150  $\mu$ M, all the studied compounds were non-cytotoxic against MCF-7.

### *In silico* pharmacokinetic study

Drug-likeness and oral absorption prediction of the synthesized compounds **7a–l** were calculated with QikProp module of Schrodinger.

Table 2 shows the descriptor values affecting the drug-likeness according to the Lipinski rule of five. It is considered that all of the synthesized compounds follow of Lipinski rule of five without any deviations and therefore are drug-like.

Solubility and permeability are two main factors affecting the oral absorption of a compound in the body [27]. Table 3 depicts the descriptor values which influence solubility, permeability, and finally the human oral absorption [28]. It shows that all the synthesized compounds with the exception of compounds **7k–l** are oral active.

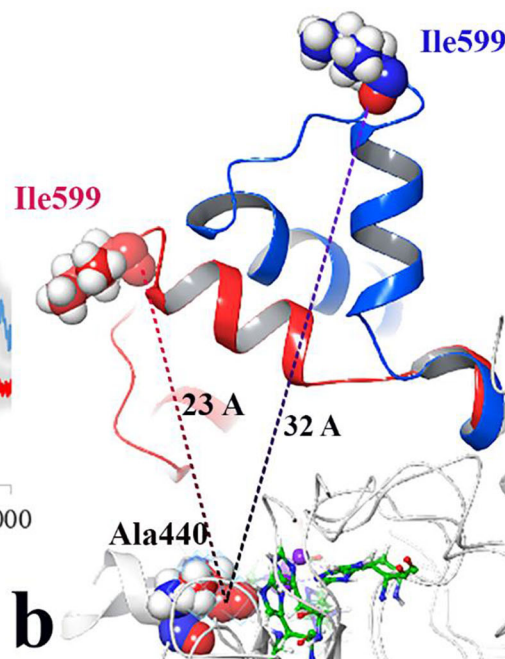
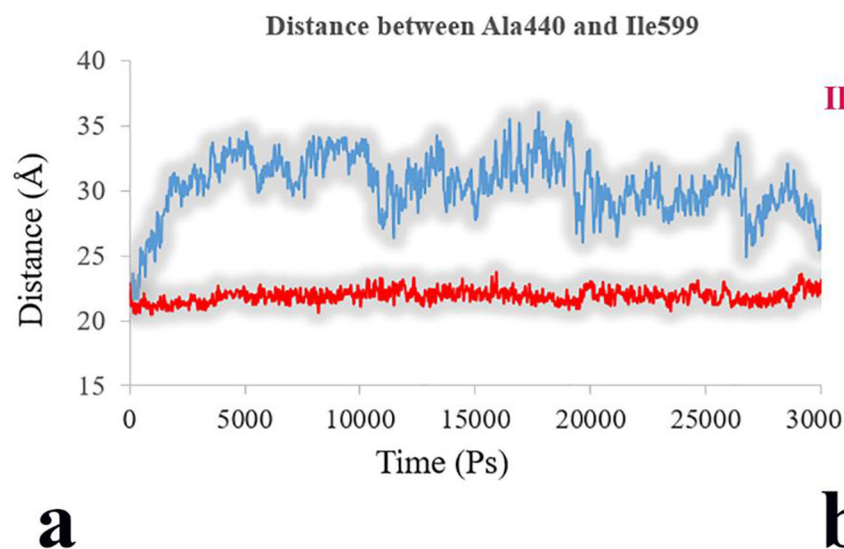


**Fig. 6** MD simulated flap distance between Ala440-Ile599 in thiourea (blue) and compound **7d** (red) in urease bound-state (**a**). Representative snapshots from MD simulations where the flap covering the active site

can adopt open conformations of the flap (blue) and closed conformation (red) (**b**). The zoom of the active site residues shows catalytic residues in green and nickel atoms in purple

**Table 2** The Lipinski rule of five properties of compounds **7a-l**

Entry	Mw	HBD <sup>a</sup>	HBA <sup>b</sup>	LogP <sub>o/w</sub> <sup>c</sup>	RBC <sup>d</sup>	Rule of five violations
<b>7a</b>	365.345	3	7.250	1.699	6	0
<b>7b</b>	383.335	3	7.250	1.926	6	0
<b>7c</b>	401.326	3	7.250	2.134	6	0
<b>7d</b>	434.235	3	7.250	2.472	6	0
<b>7e</b>	413.816	3	7.250	2.436	6	0
<b>7f</b>	381.405	3	6.750	2.811	6	0
<b>7g</b>	399.396	3	6.750	3.040	6	0
<b>7h</b>	417.386	3	6.750	3.277	6	0
<b>7i</b>	415.850	3	6.750	3.280	6	0
<b>7j</b>	450.295	3	6.750	3.694	6	0
<b>7k</b>	460.301	3	6.750	3.362	6	0
<b>7l</b>	429.877	3	6.750	3.467	6	0

<sup>a</sup> Number of average hydrogen bond donor (recommended value 0.0–6.0); <sup>b</sup> number of average hydrogen bond acceptor (recommended value 2.0–20.0); <sup>c</sup> predicted octanol/water partition coefficient (acceptable range from –2 to 6.5); <sup>d</sup> number of rotatable bond (recommended value 2.0–20.0)

## Conclusion

In conclusion, (thio)barbituric-phenoxy-*N*-phenylacetamide derivatives **7a-l** were synthesized and evaluated urease inhibitors. The obtained urease inhibitory activities showed that all the synthesized compounds were more active than standard urease inhibitors hydroxyurea and thiourea. Docking study of the synthesized compounds demonstrated that these compounds as well occupied active site cavity urease. Molecular dynamic simulation of the most active compound **7d** proposed that this compound inhibited urease by stabilizing the produced intermediate during the ureolytic reaction.

**Table 3** The calculated ADME properties of synthesized compounds **7a-l**

Entry	Log <i>S</i> <sub>wat</sub> <sup>a</sup>	PCaco <sup>b</sup>	% HOA <sup>c</sup>	Rule of three violations
<b>7a</b>	–4.087	75.181	70.469	0
<b>7b</b>	–4.435	75.192	71.802	0
<b>7c</b>	–4.758	73.215	72.814	0
<b>7d</b>	–4.947	79.827	75.466	0
<b>7e</b>	–5.064	86.673	75.895	0
<b>7f</b>	–4.965	264.691	86.768	0
<b>7g</b>	–5.316	264.740	88.112	0
<b>7h</b>	–5.698	253.405	89.156	0
<b>7i</b>	–5.520	289.660	90.216	0
<b>7j</b>	–6.099	290.358	92.657	0
<b>7k</b>	–5.808	246.436	89.448	1
<b>7l</b>	–5.755	282.585	91.118	1

<sup>a</sup> Predicted aqueous solubility in mol dm<sup>–3</sup> (–6.5–0.5); <sup>b</sup> predicted Caco-2 cell permeability in nm/s; <sup>c</sup> percentage human oral absorption (<25% is poor and >80% is high)

Furthermore, drug-likeness and oral absorption predictions of the synthesized compounds **7a-l** were performed. These studies predicted that all the synthesized compounds are drug-like and with the exception of compounds **7k-l** are oral active.

## Compliance with ethical standards

**Conflict of interest** The authors declare that they have no conflict of interest.

## References

- Sudkolai ST, Nourbakhsh F (2017) Urease activity as an index for assessing the maturity of cow manure and wheat residue vermicomposts. *Waste Manag* 64:63–66
- Modolo LV, da Silva CJ, Brandão DS, Chaves IS (2018) A minireview on what we have learned about urease inhibitors of agricultural interest since mid-2000s. *J Adv Res* 13:29–37
- Kosikowska P, Berlicki Ł (2011) Urease inhibitors as potential drugs for gastric and urinary tract infections: a patent review. *Expert Opin Ther Pat* 21:945–957
- Konturek PC, Konturek SJ, Brzozowski T (2006) Gastric cancer and helicobacter pylori infection. *J Physiol Pharmacol* 57:51
- Dunn BE, Phadnis SH (1998) Structure, function and localization of helicobacter pylori urease. *Yale J Biol Med* 71:63
- Mobley HL, Island MD, Hausinger RP (1995) Molecular biology of microbial ureases. *Microbiol Mol Biol Rev* 59:451–480
- Ikotun AA, Ojo Y, Obafemi CA, Egharevba GO (2017) Synthesis and antibacterial activity of metal complexes of barbituric acid. *Afr J Pure Appl Chem* 5:97–103
- Vosooghi M, Farzipour S, Saedi M, Shareh NB, Mahdavi M, Mahernia S, Foroumadi A, Amanlou M, Shafiee A (2015) Synthesis of novel 5-arylidene (thio) barbituric acid and evaluation of their urease inhibitory activity. *J Iran Chem Soc* 12:1487–1491
- Harris RA, Stokes JA (1982) Effects of a sedative and a convulsant barbiturate on synaptosomal calcium transport. *Brain Res* 242:157–163

10. Rahim F, Ali M, Ullah S, Rashid U, Ullah H, Taha M, Javed MT, Rehman W, Khan AA, Abid OU, Bilal M (2016) Development of bis-thiobarbiturates as successful urease inhibitors and their molecular modeling studies. *Chin Chem Lett* 27:693–697
11. Khan KM, Rahim F, Khan A, Shabeer M, Hussain S, Rehman W, Taha M, Khan M, Perveen S, Choudhary MI (2014) Synthesis and structure–activity relationship of thiobarbituric acid derivatives as potent inhibitors of urease. *Bioorg Med Chem* 22:4119–4123
12. Khan KM, Ali M, Wadood A, Khan M, Lodhi MA, Perveen S, Choudhary MI, Voelter W (2011) Molecular modeling-based anti-oxidant arylidene barbiturates as urease inhibitors. *J Mol Graph Model* 30:153–156
13. Wahid S, Jahangir S, Versiani MA, Khan KM, Salar U, Ashraf M, Farzand U, Wadood A, Taha M, Perveen S (2020) Atenolol thio-urea hybrid as potent urease inhibitors: design, biology-oriented drug synthesis, inhibitory activity screening, and molecular docking studies. *Bioorg Chem* 94:103359
14. Abbasi MA, Hassan M, Siddiqui SZ, Raza H, Shah SA, Seo SY (2018) Synthesis, in vitro and in silico studies of novel potent urease inhibitors: N-[4-({5-[(3-un/substituted-anilino-3-oxopropyl)sulfanyl]-1, 3, 4-oxadiazol-2-yl} methyl)-1, 3-thiazol-2-yl] benzamides. *Bioorg Med Chem* 26:3791–3804
15. Asadi M, Mahdavi M, Mahernia S, Rezaei Z, Safavi M, Saeedi M, Amanlou M (2018) Synthesis and urease inhibitory activity of some 5-aminomethylene Barbituric/Thiobarbituric acid derivatives. *Lett Drug Des Discov* 15:428–436
16. Moghimi S, Goli-Garmroodi F, Allahyari-Devin M, Pilali H, Hassanzadeh M, Mahernia S, Mahdavi M, Firoozpour L, Amanlou M, Foroumadi A (2018) Synthesis, evaluation, and molecular docking studies of aryl urea-triazole-based derivatives as anti-urease agents. *Arch Pharm* 351:1800005
17. Azizian H, Nabati F, Sharifi A, Siavoshi F, Mahdavi M, Amanlou M (2012) Large-scale virtual screening for the identification of new helicobacter pylori urease inhibitor scaffolds. *J Mol Model* 18: 2917–2927
18. Schrodinger LL (2012) Schrodinger suite 2012 induced fit docking protocol; glide version 5.8. Schrodinger, LLC, New York
19. Schrödinger Release 2018–4: Schrödinger Release 2018–4 Protein Preparation Wizard; Epik, Schrödinger, LLC, New York, NY, 2016; Impact, Schrödinger, LLC, New York, NY, 2016; Prime, Schrödinger, LLC, New York, 2019
20. Schrödinger Release 2018–4: LigPrep, Schrödinger, LLC, New York, 2018
21. Schrödinger Release 2018–4: Induced Fit Docking protocol; Glide, Schrödinger, LLC, New York, NY, 2018; Prime, Schrödinger, LLC, New York, 2018
22. Schrödinger Release 2018–4: Prime; MM-GBSA, Schrödinger, LLC, New York, 2018
23. Mohammadi-Khanaposhtani M, Fahimi K, Karimpour-Razkenari E, Safavi M, Mahdavi M, Saeedi M, Akbarzadeh T (2019) Design, synthesis and cytotoxicity of novel coumarin-1, 2, 3-triazole-1, 2, 4-oxadiazole hybrids as potent anti-breast cancer agents. *Lett Drug Des Discov* 16:818–824
24. Schrödinger Release 2018–4: QikProp, Schrödinger, LLC, New York, 2018
25. Ha NC, Oh ST, Sung JY, Cha KA, Lee MH, Oh BH (2001) Supramolecular assembly and acid resistance of helicobacter pylori urease. *Nat Struct Mol Biol* 8:505–509
26. Arqué X, Romero-Rivera A, Feixas F, Patiño T, Osuna S, Sánchez S (2019) Intrinsic enzymatic properties modulate the self-propulsion of micromotors. *Nat Commun* 10:1–2
27. Van De Waterbeemd H, Gifford E (2003) ADMET in silico modeling: towards prediction paradise? *Nat Rev Drug Discov* 2:192–204
28. Jorgensen WL, Duffy EM (2002) Prediction of drug solubility from structure. *Adv Drug Deliv Rev* 54:355–366

**Publisher's note** Springer Nature remains neutral with regard to jurisdictional claims in published maps and institutional affiliations.